

IDENTIFICATION OF DYNAMIC CHARACTERISTICS OF THE TSURUMI TSUBASA BRIDGE BY FIELD VIBRATION TESTS

Hiroki YAMAGUCHI¹, Haruo TAKANO², Masafumi OGASAWARA³,
Tetsushiro SHIMOSATO⁴, Masashi KATO⁵ and Jun OKADA⁶

¹ Member of JSCE, Dr. of Eng., Professor, Faculty of Engineering, Dept. of Construction Engineering, Saitama University (Ohkubo 255, Urawa, Saitama Prefecture 338, Japan)

² Member of JSCE, M. of Eng., Manager, Design Section, Kanagawa Construction Bureau, The Metropolitan Expressway Public Corporation (Masuna-cho 2-25, Naka-ku, Yokohama, Kanagawa Prefecture 231, Japan)

³ Member of JSCE, Design and Technology Section, Construction Dept., The Metropolitan Expressway Public Corporation (Kasumigaseki 1-4-1, Chiyoda-ku, Tokyo 100, Japan)

⁴ Member of JSCE, M. of Eng., Kanagawa Construction Bureau., The Metropolitan Expressway Public Corporation (Masago-cho 2-25, Naka-ku, Yokohama, Kanagawa, 231, Japan)

⁵ Member of JSCE, M. of Eng., Civil & Build. Res. Dept., Applied Tech. Res. Center, NKK Corporation, (Minamiwatarida-cho 1-1, Kawasaki-ku, Kawasaki, Kanagawa Prefecture 210, Japan)

⁶ Member of JSCE, M. of Eng., Applied Tech. Res. Center., NKK Corporation (Minamiwatarida-cho 1-1, Kawasaki-ku, Kawasaki, Kanagawa Prefecture 210, Japan)

Full-scale vibration tests on the world's longest single-plane-supported cable-stayed bridge identified various dynamic vibration characteristics. Identification methods and their suitability were examined. Ambient vibration tests illustrated the effects of the various vibration modes, the effects of boundary conditions on frequency evaluations, and the importance of amplitude range in evaluating damping. Further, forced vibration tests indicated that non-linearities seen in damping during free vibration tests can to some degree be taken into account by the modal circle fitting method. The factors influencing the low-frequency, high-damping characteristics of this bridge are compared with those of similar bridges.

Key Words: *Tsurumi Tsubasa Bridge, cable-stayed bridge, full-scale dynamic testing, natural frequency, structural damping, identification*

1. INTRODUCTION

Recent rapid progress and innovation in material science, design and construction technology has led to a large number of long-span bridges being constructed. Since bridge becomes more and more flexible as its span increases, it is necessary to carry out studies on aerodynamic and aseismic stability. Important design parameters in such studies are dynamic characteristics such as natural frequency, natural vibration mode, and structural damping factor. Of these, determining the natural frequency and natural vibration mode with relatively high accuracy has become possible. However, it is still difficult to estimate the structural damping factor quantitatively and

This paper is translated into English from the Japanese paper, which originally appeared on J. Struct. Mech. Earthquake Eng., JSCE, No.543/I-36, pp. 247-258, 1996.7.

theoretically¹⁾.

Given this background, some full-scale field vibration measurements have been conducted on actual bridges to validate the dynamic parameters assumed at the design phase. The reliability of these measurements varies depends on the experimental and analytical methods used. In particular, structural damping parameters are important to the wind-resistant design of bridges, but they are affected in many cases by a range of factors²⁾. They, therefore, need to be handled with the greatest care.

In Japan, many full-scale bridge vibration tests have been reported since the vibration tests using large vibration shakers on the Ohnaruto Bridge³⁾. Principal among them are tests on Honshu-Shikoku Bridges including the Ohshima Bridge⁴⁾, the Hitsu Ishi Jima Bridge⁵⁾, the Minami Bisan Seto Bridge⁶⁾, the Ikuchi Bridge⁷⁾, and the main bridges on the Metropolitan Expressway system, including the

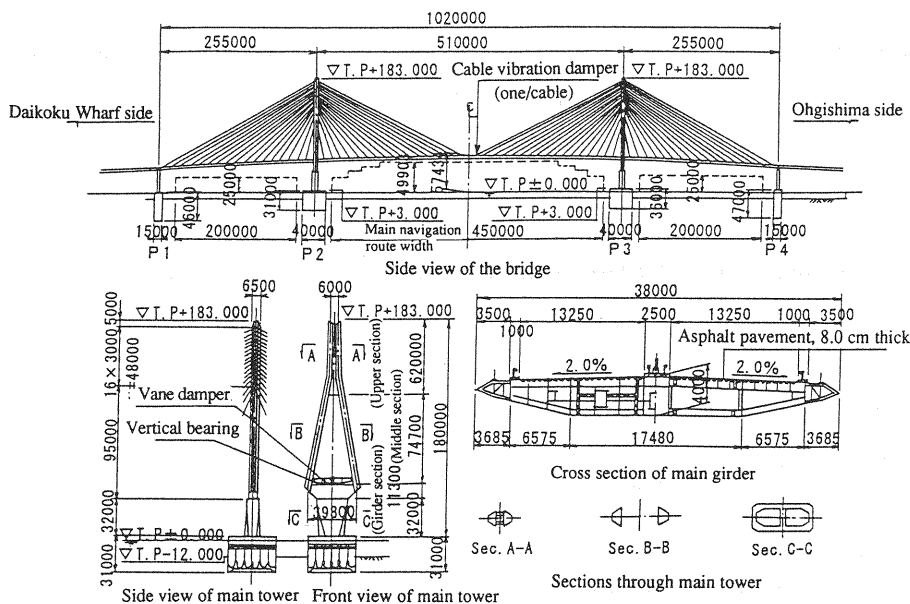


Fig. 1 General drawings of the Tsurumi Tsubasa Bridge

Yokohama Bay Bridge⁸⁾ and the Rainbow Bridge⁹⁾. However, these reports have focused mainly on (1) the validation of design, (2) clarifying the dynamic characteristics, and (3) collecting data for the design of long-span bridges in the future. This has led to insufficient discussion of variations in accuracy and reliability in identifying dynamic characteristics by experimental and analytical methods.

With the above in mind, in present study, an analysis is carried out with the results of full scale field vibration tests on the Tsurumi Tsubasa Bridge, a long-span cable-stayed bridge. We examine methods of identifying the dynamic characteristics of long-span bridges from measurements and discuss the dynamic characteristics of the bridge.

2. TSURUMI TSUBASA BRIDGE

Fig. 1 presents the general drawings of the Tsurumi Tsubasa Bridge, which forms the main link between Daikoku Wharf and Ohgishima Island on the Metropolitan Expressway system. The bridge is a three-span single-plane-supported cable-stayed steel bridge with a center span of 510 m and side spans of 255 m. The main girder are of flat box girder designed with good aerodynamic performance, and the main tower is reverse Y-shaped with a trapezoidal cross section for a slender exterior appearance.

From a structural viewpoint, the bridge is featured by elastically restrained cables. The

relative longitudinal displacement between the main girder and tower, which is linked by vertical bearings, is restrained with these cables. This contrasts with the Yokohama Bay Bridge, where the vibration isolation design is adopted. The concept is that the period of longitudinal vibrations of the main girder is significantly increased with the tower links. Vane dampers are installed on the horizontal beams of the main tower to restrain longitudinal displacement of the main girder, give stability to elastically restrained cables even during earthquakes, and add damping in the longitudinal direction. In addition, to reduce vortex-induced and rain-induced vibrations, cable dampers consisting of high-damping rubbers and oil dampers are attached to the 68 main cables. The details of the cable dampers, vertical bearings, and vane dampers are reported in Reference 10).

3. FIELD VIBRATION TESTS

(1) Specifications of vibration shakers

Large shakers owned by the Honshu-Shikoku Bridge Authority (and specified for the Oshima Bridge) were used for the field vibration tests on the bridge. These shakers of the inertial-excitation type operate as follows: the turning force from a DC motor is transmitted, via reducers, a clutch, and gears, to a crank shaft; the crank shaft links to a connecting rod, which drives a reciprocating set of weights in a vertical direction to produce an excitation force. Two shakers with a maximum excitation force of 196 kN each were

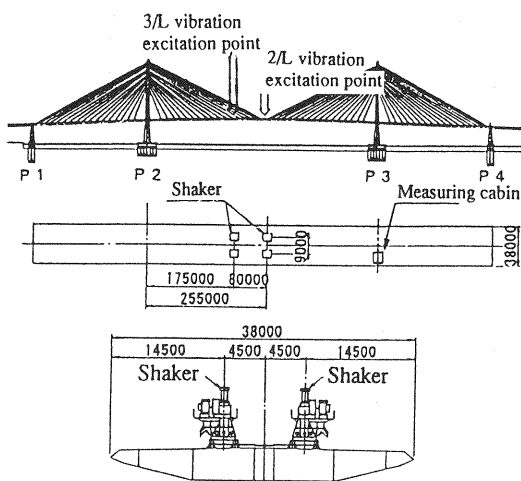


Fig. 2 Excitation positions

used to cause excitation not only in the vertical mode but also in the torsional mode. Excitation in these two modes is achieved by operating the two shakers in the same phase and out of phase, respectively. The maximum weight per shake is 33 tons, so 66 tons is available at the maximum. The minimum weight is 6 tons when the shaker is unloaded. Exciting frequencies from 0.154 to 0.920 Hz are available.

(2) Excitation modes and position

Taking into consideration the performance of the shakers, the possible excitation directions, and the schedule available for experiments, the following five vibration modes were selected:

- Two vibration modes important in the evaluation of flutter characteristics for wind-resistant design, i.e. the first sym. vertical bending and first sym. torsional modes;
- Three vibration modes, i.e. the first asym. vertical bending, second sym. vertical bending, and second asym. vertical bending modes

The field tests did not cover horizontal bending and longitudinal (like swinging-log) modes, but rather the vertical bending modes shown to be important in wind tunnel tests using a full bridge model and in time-history response seismic analysis carried out in advance of the tests.

The excitation positions are shown in Fig. 2. Vibrations were first excited in the asym. vertical bending mode at a point one-third of the way along the central span, and then in the sym. vertical bending and torsional modes after moving shakers to the center of the central span.

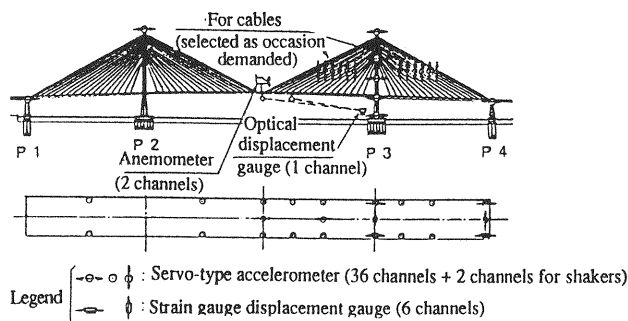


Fig. 3 Layout of measuring instruments

(3) Test methods

Kato et al.¹¹⁾ have categorized the methods of field vibration tests on actual bridges according to the characteristics of the vibrations they measured and analyzed. The following three test methods were adopted in this study:

a) Ambient vibration test

To obtain a rough understanding of natural frequency, vibration mode, and modal damping over a small amplitude range, microtremors were measured at night prior to the forced vibration test. Sensors were first placed in a vertical orientation to measure microtremors in the vertical bending and torsional modes, and then in a horizontal direction to measure microtremors in the horizontal bending mode.

b) Forced vibration test

Using the ambient vibration test as reference, as well as the results of a natural frequency analysis, stationary amplitudes were measured while changing the vibration excitation frequency in a step-by-step manner close to the natural frequency of each vibration mode. Data was collected once it was confirmed that the bridge had reached a steady vibration state. The resonance frequency, vibration mode, and modal damping were identified from the collected data.

c) Free vibration test

Free vibration waveforms were measured when the shakers were brought to a sudden stop after exciting the bridge at each resonance frequency obtained in the forced vibration test. To improve accuracy in identifying the damping characteristics, these measurements were repeated three times or more in each vibration mode.

(4) Measurements

Fig. 3 shows the layout of measuring instruments in the forced vibration and free vibration tests. For the ambient vibration tests, the instruments were laid out in the same manner but the sensors

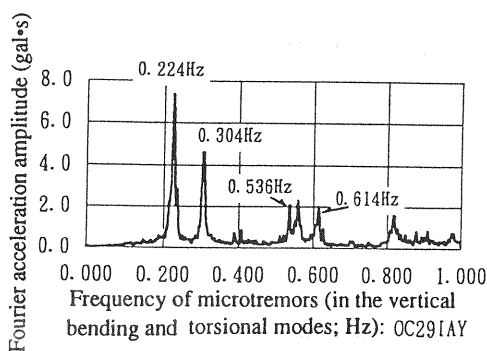


Fig. 4 Typical acceleration spectrum obtained in the ambient vibration test

were moved as required. The measured items were exciting force, girder, tower, and cable accelerations, displacement at bearings, wind direction, wind velocity, and ambient temperature at the bridge. Data were collected in the data recorders. Data on some of the measuring channels were processed on site using a simplified method to check whether the tests were being successfully implemented.

4. ANALYSIS OF TEST DATA

(1) Analysis of ambient vibration test data

The time-history response series analog data collected during the ambient vibration test was filtered using a 1 Hz low-pass filter to remove unnecessary high-frequency components. It was then digitized and FFT-processed to obtain response power spectrum. The number of FFT-processed data was 16,384 and the sampling interval was 100 ms, thus the frequency resolution was 0.0006 Hz. The sampling duration was 168 seconds. Fig. 4 shows a typical acceleration power spectrum obtained by this method. The modal damping was calculated from the peak of this power spectrum by the half-power method¹²⁾. Since simultaneous data were obtained at each measuring point, the natural vibration mode was determined by examining the amplitude ratio and phase (isophase or opposite phase) at all other measuring positions for one particular reference point.

(2) Analysis of forced vibration test data

The excitation force was calculated from the product of acceleration measured using an accelerometer attached to the shaker weight and the mass of the weight. Since the shakers were

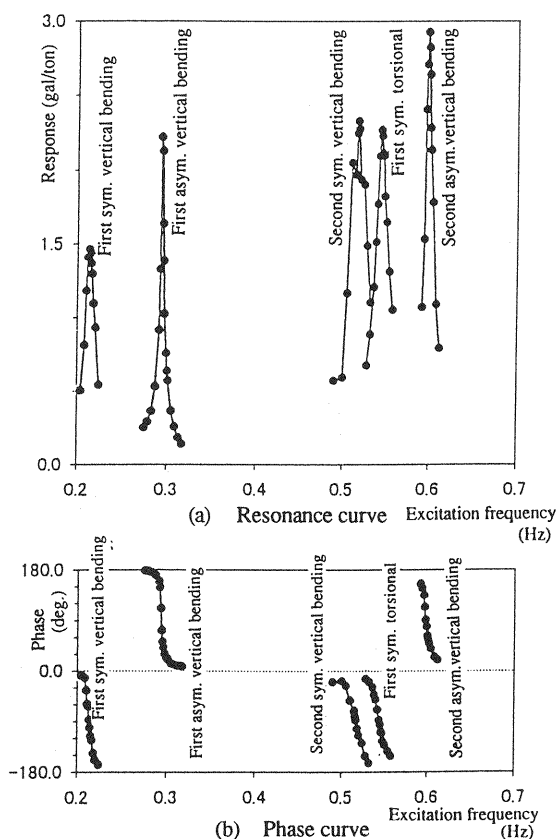


Fig. 5 Resonance and phase curves obtained from the forced vibration test

mounted on the bridge, the measured accelerations included those due to bridge vibrations. Therefore, to improve the accuracy of the analysis, the acceleration due to these vibrations was removed to obtain the actual excitation force. Control frequencies with a resolution of 0.001 Hz were adopted as excitation frequencies.

To identify the dynamic characteristics obtained in the forced vibration test, two analytical methods were used, one utilizing a resonance curve and the other the modal circle fitting method. The following is a discussion on the difference in identification accuracy between the two methods.

a) Resonance curve method

Fig. 5 shows resonance and phase curves (diagrams) for the five vibration modes. The horizontal axis represents excitation frequency, and the vertical axes are acceleration amplitude per unit excitation force, and the difference in phase between acceleration waveforms at a measuring point and at the shaker, respectively. The natural frequency was obtained from the peak of the

resonance curve, and the modal damping was extracted by the half-power method. A natural vibration mode diagram was obtained by comparing the amplitude ratio of resonance curve and phase of arbitrary points with those selected as a reference point.

b) Modal circle fitting method

Generally, frequency response functions such as compliance can be expressed approximately by circles on a Nyquist diagram if the damping is relatively small and coupling between modes is not so large. Taking advantage of this characteristic, the natural frequency and modal damping can be identified from forced vibration test data by fitting a single-degree-of-freedom curve¹³⁾. This method is outlined below.

Since many accelerometers were used in the experiments on the bridge, an acceleration, $L(f)$, representing the transfer function for the response between external excitation forces and accelerations can be used as defined below.

$$L(f) = \frac{-\frac{1}{m}\left(\frac{f}{f_n}\right)}{1 - \left(\frac{f}{f_n}\right)^2 + j\frac{\delta}{\pi}\left(\frac{f}{f_n}\right)^2} \quad (1)$$

where m = modal mass; f = excitation frequency; f_n = natural frequency in vibration mode; δ = logarithmic decrement; and j = imaginary operator.

Theoretically, the relationship between the real and imaginary part of the acceleration is represented as a circle, called a modal circle, in the complex plane of a Nyquist diagram. Experimentally, the acceleration at a particular excitation frequency can be obtained by measuring the steady-state response acceleration at that frequency. When plotting the relationship between the real part, x_i , and the imaginary part, y_i , of the acceleration obtained experimentally on a Nyquist diagram, the result is not necessarily fitted on the modal circle. (See Fig. 6 (a).) That is, there may be various errors in the measurements. Thus the data is fitted so as to minimize the square of the errors. More concretely, the equation of a modal circle is written as follows.

$$x_i^2 + y_i^2 - ax_i - by_i - c = 0 \quad (2)$$

Therefore, the coefficients of the fitted circle, a , b , and c , are given by the following equation:

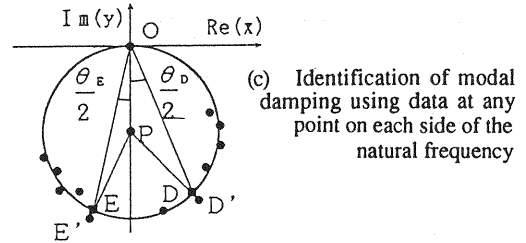
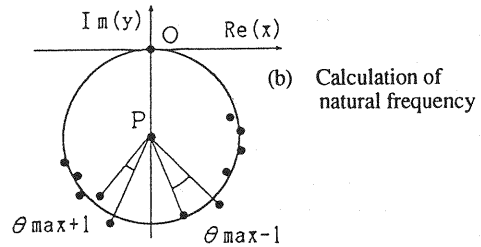
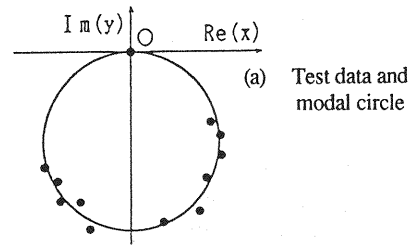


Fig. 6 Identification of the dynamic characteristics by the modal circle curve fitting method

$$\begin{Bmatrix} a \\ b \\ c \end{Bmatrix} = \begin{bmatrix} \sum x_i^2 & \sum x_i y_i & \sum x_i \\ \sum x_i y_i & \sum y_i^2 & \sum y_i \\ \sum x_i & \sum y_i & n \end{bmatrix}^{-1} \begin{Bmatrix} \sum (x_i^3 + x_i y_i^2) \\ \sum (x_i^2 y_i + y_i^3) \\ \sum (x_i^2 + y_i^2) \end{Bmatrix} \quad (3)$$

In this way, the natural frequency and modal damping are determined using the fitted modal circle. To determine a natural frequency, the center of the modal circle is first connected with measurements plotted on the diagram. The central angle formed by two adjacent two rays is set to be θ_i ($i = 1$ to $n-1$). Then the maximum central angle is found and adjacent central angles on either side of the maximum one are used to determine the natural frequency using the following equation¹³⁾:

$$f_n = f_{\max} + \frac{(f_{\max+1} - f_{\max})\theta_{\max+1}}{\theta_{\max-1} + \theta_{\max+1}} \quad (4)$$

where θ_{max} = maximum central angle, f_{max} = frequency at maximum central angle, suffix $max \pm 1$ = adjacent angle on each side of the maximum central angle. (See Fig. 6 (b).)

To determine the modal damping, the method proposed by Nagamatsu¹⁴⁾ was considered. In this method, the modal damping is determined using data at positions on each side of the natural frequency. It assumes that the data falls on the modal circle, since data measured during vibration tests on long-span bridges contain certain errors, and points do not always fall on the modal circle. Therefore, we used the two positions $D(x_D, y_D)$ and $E(x_E, y_E)$, representing intersection between the circumference of the modal circle and straight line connecting the circle center with the two points rather than the two measurement points, $D'(x'_D, y'_D)$ and $E'(x'_E, y'_E)$, as shown in Fig. 6 (c). This satisfies the assumption that the two points are on the modal circle, and $f_D = f'_D$ and $f_E = f'_E$ at the excitation frequency. In this regard, the modified modal circle fitting method presented in this paper differs somewhat from the method proposed by Nagamatsu. As a consequence, the following equation is obtained for calculating the modal damping (logarithmic damping):

$$\delta = \frac{\pi \left\{ \left(\frac{f_D}{f_n} \right)^2 - \left(\frac{f_E}{f_n} \right)^2 \right\}}{\left(\frac{f_D}{f_n} \right) \tan \frac{\theta_D}{2} + \left(\frac{f_E}{f_n} \right) \tan \frac{\theta_E}{2}} \quad (5)$$

The modal damping was calculated as described above using data at four adjacent points on each side of the natural frequency. The average of the modal damping calculated by two-point data selected as a pair of data from four-point data was taken as the modal damping. Data at four points was adopted because the calculation would have yielded errors in specific data if there were too few data points. On the other hand, the result of this method would almost equate with that of the half-power method described later if the number of data was too many. Incidentally, trial calculations were made for specific cases using data at three and five points, but results differed in no significant way from four-point case.

Fig. 7 shows modal circles drawn up using the modified method described above, and Table 1 lists the calculated average modal damping (logarithmic decrement), δ_{AVE} , minimum modal

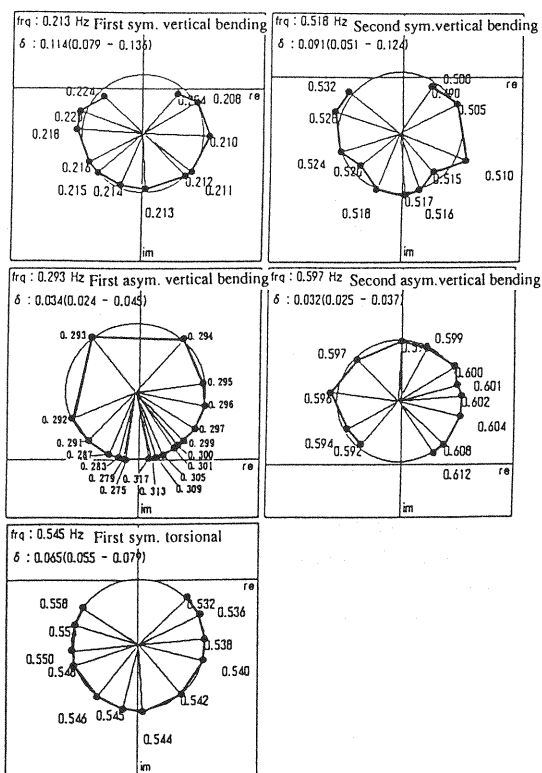


Fig. 7 Model circle curve fittings in the forced vibration tests

Table 1 Accuracy of modal damping identification by modal circle curve fitting method

| Vibration mode | δ_{AVE} | δ_{MIN} | δ_{MAX} | V |
|-----------------------|----------------|----------------|----------------|----------------------|
| First sym. Vertical | 0.11 | 0.079 | 0.140 | 2.1×10^{-4} |
| First asym. Vertical | 0.03 | 0.024 | 0.045 | 4.2×10^{-5} |
| First sym. Torsional | 0.07 | 0.055 | 0.079 | 4.1×10^{-5} |
| Second sym. Vertical | 0.09 | 0.051 | 0.120 | 3.8×10^{-4} |
| Second asym. Vertical | 0.03 | 0.025 | 0.037 | 1.0×10^{-5} |

damping, δ_{MIN} , maximum modal damping, δ_{MAX} , and variance, V .

The reliability of the average modal decrement, δ_{AVE} , can be evaluated from the variance, V in this method. As listed in Table 1, the variance in the first asym. vertical bending, first sym. torsional, and second asym. vertical bending modes are of the order of 10^{-5} , whereas those in the first and second sym. vertical bending modes are larger by one

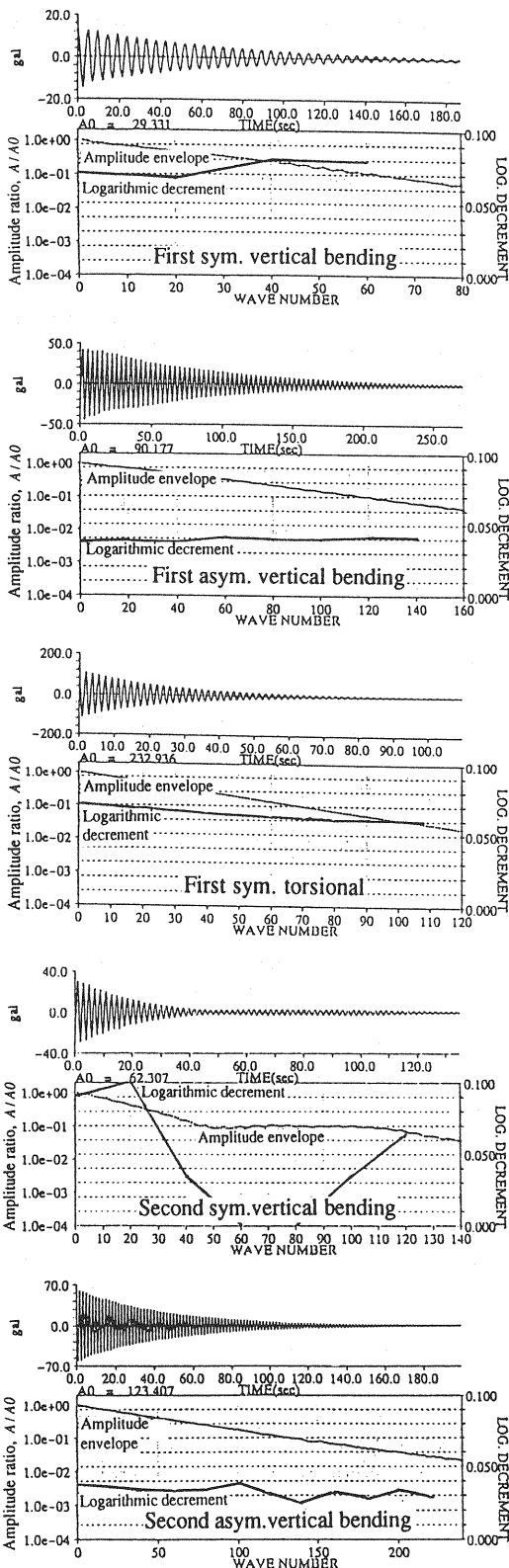


Fig. 8 Free vibration waveforms, the wave number versus amplitude envelope, and wave number versus logarithmic decrement

order of magnitude, thus indicating a slightly poor fitting to the modal circle.

(3) Analysis of free vibration test data

The time-history response series analog data collected in the free vibration test was filtered using a 1 Hz low-pass filter before conversion into a digital signal. To prevent problems with accuracy at micro-amplitude levels, an A/D converter with a 14-bit resolution was used to capture the data.

Fig. 8 shows free vibration waveforms, wave number versus amplitude envelope, and the wave number versus logarithmic decrement. In the graph showing free vibration waveforms, the horizontal and vertical axes are time in seconds and acceleration amplitude in gal, respectively. The axes of the wave number versus amplitude envelope graph are the wave number (counted as two waves per cycle) and amplitude ratio (A/A_0 = a ratio of arbitrary double-amplitude, A , to maximum double-amplitude, A_0) respectively. In the graph showing the wave number versus logarithmic decrement, the horizontal and vertical axes are the wave number and logarithmic decrement, δ , respectively.

The peak method¹²⁾, by which the peak-to-peak period of a series of waves is extracted, was used to calculate the natural frequency. For logarithmic decrement, an average of values from the first to the tenth cycles was taken. As described above, to check repeatability, measurements were repeated consecutively three times or more in each vibration mode.

5. COMPARISON AND DISCUSSION OF METHODS FOR IDENTIFYING DYNAMIC CHARACTERISTICS

(1) Natural frequency

Table 2 compares the values of natural frequency identified by the vibration tests. The frequencies given as identified by eigenvalue analysis in the table were obtained using a space-frame model. In this model, the functionality of bearings at end sections and at supporting sections of the girder on the towers were faithfully modeled. Beam elements were used to represent girders and towers, rod elements that transfer only axial forces and torque for cables. The substructure was assumed to be fixed at the top of the bridge pier.

As shown in Table 2, almost the same results were derived from the forced vibration test data by

Table 2 Comparison of identified natural frequencies

| Vibration mode | Spectrum by ambient vibration test | Forced vibration test | | Free vibration peak method | Eigenvalue analysis *1) |
|-----------------------|------------------------------------|-----------------------|--------------|----------------------------|-------------------------|
| | | Resonance curve | Modal circle | | |
| First sym. Vertical | 0.224 | 0.213 | 0.213 | 0.213 | 0.210 |
| First sym. Horizontal | 0.304 | — | — | — | 0.253 |
| First asym. Vertical | 0.316 | 0.293 | 0.293 | 0.293 | 0.290 |
| First sym. Torsional | 0.558 | 0.544 | 0.545 | 0.545 | 0.501 |
| Second sym. Vertical | 0.536 | 0.517 | 0.518 | 0.516 | 0.512 |
| Second asym. Vertical | 0.614 | 0.598 | 0.597 | 0.599 | 0.597 |

*1) One rod element per cable

At vertical bearings, longitudinal sliding is allowed.

both the resonance curve and modal circle fitting methods, as well as from the free vibration test data by the peak method. This demonstrates that there is little difference among these methods of identifying the natural frequency, and that natural frequencies are identified with good accuracy.

In one case only, the natural frequencies identified from the ambient vibration test, the frequencies were larger than those identified from the other tests by 3% to 5%. Good agreement was obtained among the natural frequencies identified by eigenvalue analysis and the forced vibration and free vibration tests, though in the first sym. torsional mode the natural frequencies identified from forced vibration and free vibration data were larger than those identified by eigenvalue analysis, with a discrepancy of nearly 9%.

To look into the differences between natural frequency values identified from experimental data and from the eigenvalue analysis, the analytical model used to determine the natural frequencies was partly changed. The results are listed in **Table 3**. In Model I, cables are replaced by a three-mass system that takes into account the tensile force in the cable by means of a shear spring. Frequencies in the bending modes increased slightly because of the effects of tensile rigidity of cables. In particular, the natural frequency in the second sym. vertical bending

mode, where strong coupled vibrations were observed in the cables, approached somewhat closer to that obtained in the forced vibration and free vibration data, when compared with the natural frequency obtained from the eigenvalue analysis listed in **Table 2**. However, in the first sym. torsional mode, where the largest difference between natural frequencies obtained from the eigenvalue analysis and those from the forced vibration and free vibration tests is seen, there is little difference in the natural frequency despite this change in the model. A discussion of the natural frequency in the torsional mode is given below.

When a bridge girder undergoes torsional rotation, the rotation center of the girder is lower than the anchor point of the single-plane-supported cables on the girder side, so thus the cable is subject to an out-of-plane deformation. Accordingly, we estimate that the natural frequency would increase, because the rigidity of the cable due to the introduced tensile force would be added to the torsional rigidity of the girder. However, there was no effect on the natural frequency in the torsional mode. This may be due to the small out-of-plane component of the cable.

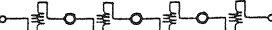
Incidentally, since the actually measured rotation center is at a point higher than assumed in the design phase, an additional study was carried out correcting the polar moment of inertia with consideration of this difference in vertical elevation. As a result, the natural frequency increased by 1.3% but the difference of 9% could not be eliminated. A further study investigated into the effects on torsional frequency of the spring stiffness of the high-damping rubber fitted about 2 m away for the girder's rotation center.


Without the need for an eigenvalue analysis, it was possible to show that there was no increase in general stiffness and that the effect of the rubber's spring stiffness was negligible. This clarifies that these factors are not leading causes of the torsional frequency obtained in eigenvalue analysis being lower than the experimental values. Instead, other factors such as the effects of secondary members, which were not taken into account in the analysis, are likely to be the cause. However, it has not yet been determined clearly.

The frequencies listed in the Model II column of **Table 3** are those obtained when the longitudinal restraint conditions at vertical bearings were changed from sliding to fixed. These frequencies are somewhat closer to those obtained in the ambient vibration tests. During the forced vibration and free vibration tests, the bearings

Table 3 Comparison of natural frequencies for different analytical models

| Vibration Mode | Natural frequencies obtained from eigenvalue analysis | |
|----------------------|---|------------|
| | Model I* | Model II** |
| First sym. Vertical | 0.218 | 0.228 |
| First sym.horizontal | 0.258 | 0.318 |
| First asym. vertical | 0.296 | 0.309 |
| First sym. Torsional | 0.501 | 0.501 |
| Second sym.vertical | 0.520 | 0.526 |
| Second asym.vertical | 0.611 | 0.598 |

* Cable model (Model I) 

** Cable model (Model II) 

overcame inherent friction forces and sliding occurred. During the ambient vibration test, the amplitude was not so large as the bearings could slide. Strong restraint in the longitudinal direction seems to be one reason for the natural frequencies identified in the ambient vibration tests being higher than those in the other tests.

(2) Natural vibration modes

In Fig. 9, the natural vibration modes identified by eigenvalue analysis, the ambient vibration tests, and the forced vibration tests are compared. Apart from a slight difference in the first asym. vertical bending mode at the towers, these values are in good agreement; this includes the first sym. horizontal bending mode that was obtained only in the ambient vibration test. This demonstrates that vibration modes can be obtained with satisfactory accuracy even from ambient vibration tests, at least in the case of this bridge.

(3) Modal damping factor

Table 4 offers a comparison of the identified modal damping (logarithmic decrements). Values identified from the ambient vibration test differ from those obtained from other tests. Given that the maximum amplitude in the ambient vibration test was very small, as listed in Table 4, and that external perturbations were assumed to be white noise when analyzing the data, it seemed difficult to compare modal damping in this simplified manner. Accordingly, for four of the vibration modes — leaving out the second sym. vertical bending mode where coupled vibrations occurred — logarithmic decrement in the small amplitude region were obtained from the relationship between the wave number and the logarithmic decrement

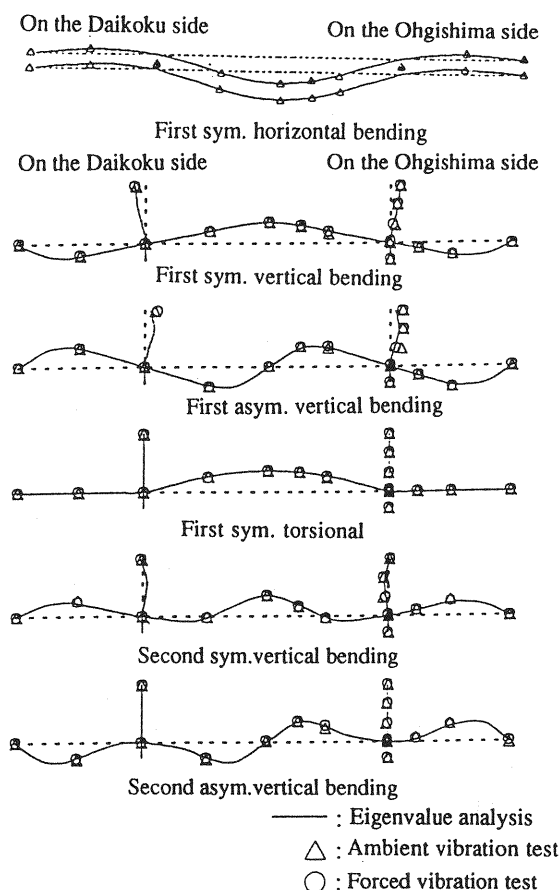


Fig. 9 Comparison of natural vibration modes

shown in Fig. 8, and they were then compared with the damping identified in the ambient vibration test. For the first sym. vertical bending mode, it identified logarithmic decrement of $\delta = 0.09$, whereas that obtained from Fig. 8 is $\delta = 0.08$. Similarly, in the first asym. vertical bending mode, the identified value was $\delta = 0.07$, whereas that obtained from Fig. 8 is $\delta = 0.04$. In the first sym. torsional mode, the identified value was $\delta = 0.05$ as compared with $\delta = 0.06$. In the second asym. vertical bending mode, both the identified and obtained values were $\delta = 0.03$. Thus the identified damping factors for all modes were close to the values in the small amplitude region of, as compared with the factors listed in Table 4. This indicates that, in the evaluation of structural damping, it is preferable to compare damping factors identified in the micro-amplitude region of a free vibration test with those identified in an ambient vibration test. Next is the adequacy of methods of identifying damping on a modal circle using forced vibration test data by comparing the

Table 4 Comparison of identified modal dampings

Values in parentheses indicate maximum amplitudes.**
 Values in the torsional mode are in degrees

| Vibration mode | Modal damping (logarithmic decrement) | | | |
|-----------------------|---------------------------------------|--|---|---------------------|
| | Ambient vibration test | Forced vibration test Modal circle fitting method | | Free vibration test |
| | Half-power method | Half-power method | Modified modal circle curve fitting method*1) | |
| First sym. vertical | 0.09 (0.55) | 0.12 (8.8) | 0.11 (8.8) | 0.07 (8.2) |
| First asym. vertical | 0.07 (0.017) | 0.03 (14.5) | 0.03 (14.5) | 0.04 (13.4) |
| First sym. torsion | 0.05 (0.003) | 0.07 (0.43) | 0.07 (0.43) | 0.07 (0.38) |
| Second sym. vertical | 0.03 (0.004) | 0.11 (3.2) | 0.09 (3.2) | 0.10*** (3.0) |
| Second asym. vertical | 0.03 (0.002) | 0.03 (4.6) | 0.03 (4.6) | 0.04 (4.2) |

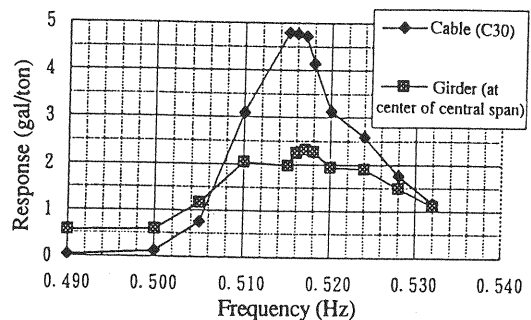
* Method of calculating modal damping from any point on each side of the natural frequency

** Maximum amplitudes in cm.

In the ambient vibration test, displacement amplitudes converted from Fourier acceleration amplitudes in mm.

*** Cables resonated with this mode and beating occurred.

results with factors identified in free vibration tests. In the first asym. vertical bending, second asym. vertical bending, and first sym. torsional modes, where the variance is less than other in modes as listed in **Table 1**, and roughly the same damping was obtained from the forced vibration data by the half-power method and the modified modal circle fitting method and from the free vibration data. (See **Table 4**.) The fact that the variance is small and the fitting to the modal circle is good means that these vibration modes are close to the response of a single-degree-of-freedom system and the amplitude dependence of damping is small. Actually, **Fig. 8** clearly shows that the amplitude dependence is relatively small and the variance is small. That is, variance can be taken as a standard by which to measure the reliability of identified damping. The smaller the variance, the smaller the amplitude dependence of damping. It is confirmed that there is approximate agreement

**Fig. 10** Resonance curves of girders and cables

between dampings identified from forced vibration test data by the conventional half-power method, and the modified modal circle fitting method, and from free vibration data.

As regards the two vibration modes where the variance in identifying modal dampings by the modal circle fitting method was an order of magnitude greater than those of the other modes, i.e. the first and second sym. vertical bending modes, the amplitude dependence of damping are also relatively large.

The cause of this larger variance and poor fitting to the modal circle in the case of the second sym. vertical bending mode seems to be the effect of coupled vibrations during the tests. It is clear from the resonance curves of girder and cable in the second sym. vertical bending mode in **Fig. 10**, that the acceleration response of the cable was very large and the peak frequency of the cable and girder were close to each other.

The first sym. vertical bending mode, as shown in **Fig. 8**, was the only mode where the modal damping had a tendency to decrease at relatively large amplitude. The trend is also evident in the damping identified from the forced vibration data by the modified modal circle fitting method, as given in **Table 4**. This indicates that the damping obtained by the modified method — that is, using only data of relatively large amplitude adjacent to the natural frequency on the modal circle — was slightly smaller than that obtained by the conventional half-power method corresponding to calculate the damping from all data on the modal circle. It does not change, even when the number of points on the circle is three or five. In other words, there is a possibility that a logarithmic decrement calculated by modified method is close to the peak frequency on the modal circle even when the amplitude dependency of structural damping is strong.

In the case of the second sym. vertical bending

mode, the damping is an apparent value because beating arose when girder and cables resonated during the free vibration test. Consequently, it is difficult to judge whether the modified modal circle fitting method can take into account non-linearity in damping amplitudes. On the other hand, in the first sym. vertical bending mode, the difference between the damping identified from the free vibration test data is 0.07, and that identified from the modified modal circle fitting method is 0.11. How to handle these data is an important issue in identifying logarithmic decrement from test data collected for long-span bridges.

6. DYNAMIC CHARACTERISTICS OF THE TSURUMI TSUBASA BRIDGE

In the previous section, methods of identifying dynamic characteristics from full-scale vibration tests were discussed. It was concluded that natural frequency and modal damping could be identified from free vibration data with considerable accuracy. Based on these identified values, we now discuss the dynamic characteristics of the Tsurumi Tsubasa Bridge.

(1) Natural frequency

Fig. 11 shows the relationship between the lowest-mode natural frequency (fundamental frequency) and the maximum span length of cable-stayed bridges, comparing the vertical bending and torsional vibrations of the Tsurumi Tsubasa Bridge with other cable-stayed bridges^{15),16)}. The natural frequency of this single plane supported cable-stayed bridge seems to be somewhat low relative to its span, but it is approximately an extrapolation of values for other cable-stayed bridges plotted in the figure.

Of the bridges plotted, the one closest in span to the 510 m of the Tsurumi Tsubasa Bridge is the Ikuchi Bridge, with a span of 490 m. We will focus on the dynamic characteristics of these two cable-stayed bridges. The natural frequency of the Tsurumi Tsubasa bridge is much lower than that of the Ikuchi Bridge. Bending and torsional rigidity are two to three times the values for the Ikuchi Bridge. In terms of weight, it is heavier than the Ikuchi Bridge by only about 20%, so there is not such a sharp contrast as in the rigidity. Considering this relation between rigidity and weight, this bridge can be expected to show a rather higher natural frequency than the Ikuchi Bridge.

In the first sym. vertical bending mode of the

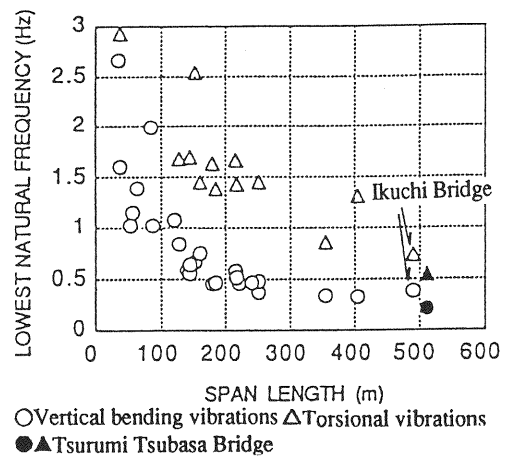


Fig. 11 Relationship between lowest frequency and span length of cable-stayed bridges

Tsurumi Tsubasa Bridge, as shown in Fig. 9, the modal component at the central span is almost the same as that of the side spans, and the vibration mode of the central span is similar to that of a simply supported beam. In contrast, since the Ikuchi Bridge has PC side spans, the vibration mode is similar to that of a beam with both ends fixed. It can be considered that the lowest natural frequency of the bridge in the first sym. vertical bending mode is due to this difference in the vibration mode arising from different restraints affected by the side spans.

In the first sym. torsional mode, on the other hand, since the vibration modes of both bridges are almost the same, the restraint conditions by the side span seems almost the same. Accordingly, in spite of the difference in torsional rigidity, the large difference in rotational stiffness due to cable differences makes the torsional frequency of this single-plane-supported bridge smaller than that of the Ikuchi Bridge.

As explained above, the natural frequency of cable-stayed bridges is affected more by the vibration mode of its girder, the restraint conditions by side spans due to differences in rigidity between the side and central spans, and the apparent rigidity due to differences in cable type than by the rigidity and weight of the girder itself. Thus the natural frequency is not necessarily dependent on the central span length.

(2) Modal damping characteristics

Fig. 12 shows the relationship between natural frequency and modal damping for cable-stayed bridges in the case of vertical bending and torsional

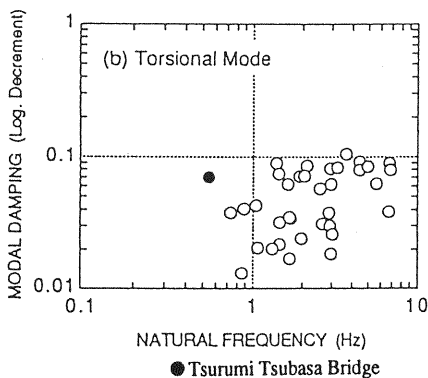
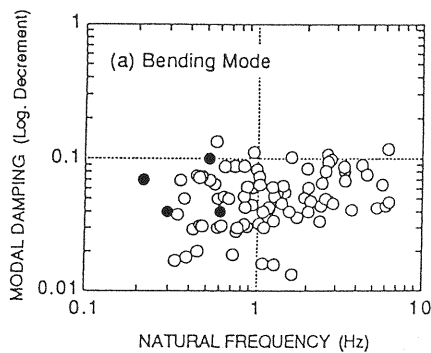


Fig. 12 Relationship between natural frequency and modal damping of cable-stayed bridges

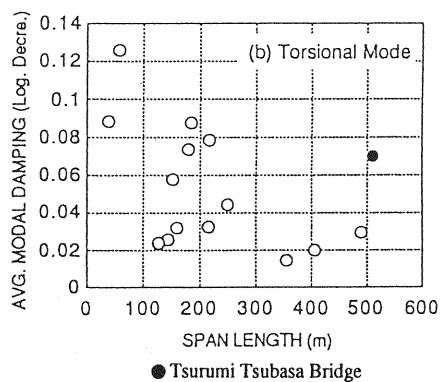
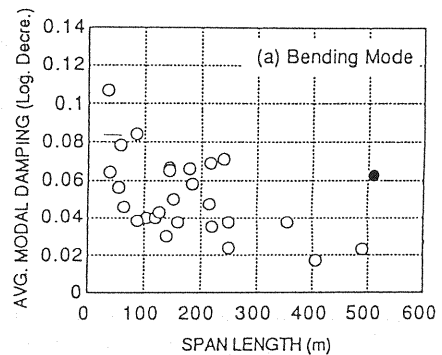


Fig. 13 Relationship between span length and average modal damping of cable-stayed bridges

vibrations; the Tsurumi Tsubasa Bridge is compared with other cable-stayed bridges. As is the case with other cable-stayed bridges¹⁶⁾, the correlation between natural frequency and modal damping is poor, indicating a strong mode-dependence of damping.

Fig. 13 shows the average modal damping in vertical bending and torsional vibrations, which are representative of the damping of cable-stayed bridges, plotted with respect to bridge span without regard to the order of the vibrations. Although the average dampings of other bridges gradually decreases as the span increases, this bridge deviates from this tendency since it has a high average damping in spite of its long span of 510 m. It is, as apparent in Table 4, due to large damping in the first sym. vertical bending and first sym. torsional modes (aside from the second sym. vertical bending mode which is accompanied by beating due to cable resonance).

In the case of first sym. vertical bending vibrations, the measurements clarified that a sliding displacement of 1 to 2 mm occurred at the vertical bearings due to longitudinal displacement of the girder when a deflection of about 8 cm was generated at the center of the central span. Assuming that the design vertical load acting on

the four vertical bearings is about 7,200 kN, the amount of dissipated energy by friction forces at the bearings is not negligible. In addition, as shown in Fig. 8, the amplitude dependence of the damping in the first sym. vertical bending mode is relatively large. The smaller the amplitude, the larger the damping. This agrees with the observations of Ito et al.²⁾ which showed that the smaller the amplitude the larger Coulomb damping was caused. It also clarifies why the effects of friction forces are large in the first sym. vertical bending mode.

On the contrary, in the first asym. vertical bending mode, the damping identified from free vibration data was 0.04, less than in the first sym. vertical bending mode, and the displacement at the bearings was small. That is, the damping in the first sym. vertical bending mode of this bridge becomes larger compared with other cable-stayed bridges of similar scale because frictional bearings were adopted instead of the usual link bearings, and the amount of dissipated energy by frictional forces is large.

In the first sym. torsional mode, although the damping is thought to be small because of a single-plane-supported bridge, it was in fact larger than those of other cable-stayed bridges of similar scale.

The primary cause of this is the large amount of energy dissipated from the cable dampers, which consist of oil dampers and high-damping rubber. In other words, in a single-plane-supported cable-stayed bridge, although the cables rarely move even when girder suffers torsional vibrations, the cable dampers mounted some distance from the girder rotation center deformed and dissipated a large amount of energy. There is no other bridge of similar scale in which cable dampers exert such a large effect on the damping of girder. Detailed discussions on the damping characteristics of the bridge are reported in Reference 17) and 18).

7. CONCLUSIONS

With the focus on the Tsurumi Tsubasa long-span cable-stayed bridge, a study has been carried out on methods of identifying dynamic characteristics such as natural frequency, natural vibration mode, and structural damping using full-scale test data from the bridge. The results of the study are summarized as follows.

- (1) Good agreement was obtained between the values of natural frequency identified from forced vibration tests by the modal circle fitting method and resonance curve method and that identified from free vibration test data by the peak method. It demonstrates that there is little difference between these three identification methods and the accuracy of the methods is high. However, the natural frequency identified from ambient vibration test data was 3% to 5% higher than the values obtained from forced vibration and free vibration test data. It is because there is no movement in a longitudinal direction at the vertical bearings during the ambient vibration tests.
- (2) It was verified that the natural vibration mode obtained from the forced vibration test agreed approximately with that calculated by eigenvalue analysis. In spite of the small amplitudes employed in the ambient vibration test, insofar as vibration mode is concerned, the accuracy of vibration mode identification was quite reasonable.
- (3) The variance in the experimental data, which indicates the degree of fitting to the modal circle, can be used as a standard by which the reliability of the identified damping can be evaluated. The modified modal circle fitting method presented in this paper indicates that the possibility of calculating the logarithmic decrement close to the peak frequency with good accuracy, even when the amplitude dependence of structural damping is strong.

(4) When the dampings identified in ambient vibration tests by the half-power method with the forced vibration and free vibration tests are compared, it should be done in the small amplitude region taking into account very small vibration levels of the ambient vibration test data.

(5) As compared to the Ikuchi Bridge, a cable-stayed bridge of similar scale, the natural frequency of the Tsurumi Tsubasa Bridge in the first sym. vertical bending and torsional modes was lower. The primary causes are relatively weak restraint at side spans during vertical bending vibrations and the low rotational rigidity of the entire bridge system due to the single-plane-supported design.

(6) The damping of the Tsurumi Tsubasa Bridge in the first sym. vertical bending and torsional modes was larger than that of other cable-stayed bridges of similar scale.

REFERENCES

- 1) Yamaguchi, H.: Damping Estimation of Cable Systems, *Journal of Structural Engineering*, JSCE, Vol. 39A, pp. 851-860, Mar. 1993 (in Japanese).
- 2) Ito, M. and Katayama, T.: Damping of Bridge Structures, *Proc. of JSCE*, No. 117, pp. 12-22, 1965 (in Japanese).
- 3) Okauchi, I., Miyata, T., Tatsumi, M., and Kiyota, R.: Dynamic Field Tests and Studies on Vibration Characteristics of Long-Span Suspension Bridges, *Proc. of JSCE*, No. 446/I-19, pp. 101-112, 1992.
- 4) Hiratsuka, Y.: Vibration Test for Aerodynamic Stability on Ohshima Bridge, *HSBA Technical Reports*, Vol. 13, No. 48, pp. 42-47, Oct. 1988 (in Japanese).
- 5) Okauchi, I., Miyata, T., Tatsumi, M., and Sasaki, N.: Vibration tests on Long-Span Bridges Using Large Amplitude Excitations, *Proc. of JSCE*, No. 455/VI-21, pp. 75-84, Oct. 1992 (in Japanese).
- 6) Okuda, M. and Okawa, M.: Vibration Test on Aerodynamic Stability of Minami Bisan Seto Bridge, *HSBA's Technical Reports*, Vol. 13, No. 49, Jan. 1989 (in Japanese).
- 7) Fujiwara, T., Tamakoshi, T., Ueda, T., Nanjo, M., and Kobayashi, Y.: Characteristics of Vibration of Complex Multi-Cable Stayed Bridge, *Journal of Structural Engineering*, Vol. 39A, pp. 831-839, Mar. 1993 (in Japanese).
- 8) Wada, K., Takano, H., Hayashi, H., Koyama, J., and Tsumura, N.: Vibration Tests of the Yokohama Bay Bridge, *Bridges and Foundations*, Vol. 26, pp. 15-18, Feb. 1992 (in Japanese).
- 9) Izumi, K., Odagiri, N., Ogiwara, M., Yabe, J., Ochiai, M., Ogaki, K., and Watanabe, Y.: Vibration Test for a Two Hinge Double-Deck Suspension Bridge, *Journal of Structural Engineering*, Vol. 40A, pp. 721-733, Mar. 1994 (in Japanese).
- 10) Takano, H., Ogasawara, M., and Shimozato, T.: Construction of the Metropolitan Expressway, No. 7: Overview of Design of Superstructures of the Tsurumi Tsubasa Bridge, *Civil Engineering Technology*, Vol. 50,

- No. 1, pp. 84-93, 1995 (in Japanese).
- 11) Kato, M. and Shimada, S.: Field Vibration testsal Methods for Bridges, *Proc. of JSCE*, Vol. 66, No. 2, pp. 38-42, 1981 (in Japanese).
 - 12) Oshima, T., Okabayashi, T., Kajikawa, Y., Kato, M., Kawatani, M., Kubo, M., Sugimoto, M., Hayashikawa, T., Honda, H., Maeda, K., and Yoneda, M.: Measurement and Analysis of Bridge Vibrations, Oct. 1993 (in Japanese).
 - 13) Nagamatsu, A.: Modal Analysis, Baifukan Publishing Co., Ltd., 1985 (in Japanese).
 - 14) Nagamatsu, A.: Guide to Modal Analysis, Corona Publishing Co., Ltd., 1993 (in Japanese).
 - 15) Ito, M. and Yamaguchi, H.: Full-scale Measurements and Structural Damping of Cable-Supported Bridges, *Proc. of Int. Conf. on Bridges Into The 21st Century*, Hong Kong, Oct. 1995.
 - 16) Yamaguchi, H.: Modal Damping of Cable Structures and Its Theory, *Proc. of Steel Structures*, Vol. 1, No. 3, pp. 129-138, Sept. 1994 (in Japanese).
 - 17) Yamaguchi, H., Kurokawa, S., Ito, N., Kato, M., and Kato, H.: Energy-Based Evaluation of Damping Characteristics of the Tsurumi Tsubasa Bridge, *The 50th JSCE Annual Conference* pp. 1012-1013, Sept. 1995 (in Japanese).
 - 18) Yamaguchi, H., Takano, H., Ogasawara, M., Shimosato, T., Kato, M., and Kato, H.: Energy-Based Damping Evaluation of Cable-Stayed Bridges and Its Application to Tsurumi Tsubasa Bridge, *Proc. of JSCE*, No. 543/I-36, pp. 217-227, July 1996 (in Japanese).